

Stochastic Quantum Spiking Neural Networks with Quantum Memory and Local Learning

Jiechen Chen^{*}, Bipin Rajendran and Osvaldo Simeone

Centre for Intelligent Information Processing Systems (CIIPS),
Department of Engineering, King’s College London, London, WC2R
2LS, UK.

^{*}Corresponding author. E-mail: jiechen.chen@kcl.ac.uk;

Contributing authors: jiechen.chen@kcl.ac.uk;
bipin.rajendran@kcl.ac.uk; osvaldo.simeone@kcl.ac.uk;

Abstract

Neuromorphic and quantum computing have recently emerged as promising paradigms for advancing artificial intelligence, each offering complementary strengths. Neuromorphic systems built on spiking neurons excel at processing time-series data efficiently through sparse, event-driven computation, consuming energy only upon input events. Quantum computing, on the other hand, leverages superposition and entanglement to explore feature spaces that are exponentially large in the number of qubits. Hybrid approaches combining these paradigms have begun to show potential, but existing quantum spiking models have important limitations. Notably, prior quantum spiking neuron implementations rely on classical memory mechanisms on single qubits, requiring repeated measurements to estimate firing probabilities, and they use conventional backpropagation on classical simulators for training. Here we propose a stochastic quantum spiking (SQS) neuron model that addresses these challenges. The SQS neuron uses multi-qubit quantum circuits to realize a spiking unit with internal quantum memory, enabling event-driven probabilistic spike generation in a single shot. Furthermore, we outline how networks of SQS neurons—dubbed SQS neural networks (SQSNNs)—can be trained via a hardware-friendly local learning rule, eliminating the need for global classical backpropagation. The proposed SQSNN model fuses the time-series efficiency of neuromorphic computing with the exponentially large inner state space of quantum computing, paving the way for quantum spiking neural networks that are modular, scalable, and trainable on quantum hardware.

Keywords: quantum neuromorphic computing, spiking neural networks, quantum machine learning, probabilistic spiking models, local learning rules.

Introduction

Neuromorphic and quantum computing have emerged as two prominent paradigms for advancing computation beyond the limits of the conventional digital CMOS transistor-based architecture^{1,2}. Each offers complementary advantages. Quantum computing leverages intrinsically quantum phenomena—mostly superposition and entanglement—to access exponentially large signal spaces with increasing numbers of qubits³⁻⁵. This massive parallelism, fundamentally inaccessible to classical systems, has recently been harnessed for machine learning^{6,7}. Neuromorphic computing, inspired by biological neural systems, implements networks of spiking neurons that communicate via discrete, asynchronous events and remain inactive in the absence of input. This sparse, event-driven mode of computation yields highly energy-efficient processing, well suited for time-series and streaming data⁸⁻¹⁰. Spiking neural networks (SNNs) also support online and continual learning, adapting to new information without retraining from scratch^{11,12}.

Given these strengths, a compelling question is whether combining quantum and neuromorphic principles can produce new models that inherit the advantages of both^{2,13}. An ideal hybrid would use quantum systems to provide exponentially large state spaces or rich dynamics, while adopting neuromorphic design to ensure robustness, sparsity, and event-driven efficiency.

Early work at this intersection has shown promise. For example, quantum reservoir computing (QRC) uses the complex dynamics of quantum systems as a temporal reservoir for processing time-dependent signals, and small quantum reservoirs have matched the performance of classical recurrent neural networks hundreds of times larger¹⁴⁻¹⁷. Another line of work aims at adapting classical spiking neuron models to quantum hardware. Notably, the quantum leaky integrate-and-fire (QLIF) neuron was recently introduced as a quantum analog of a classical spiking leaky integrate-and-fire (LIF) neuron¹³. By cascading QLIF neurons, the first quantum SNN (QSNN) was demonstrated to be capable of simple image recognition tasks such as MNIST classification¹³.

This seminal result proved the viability of spiking neural networks on quantum processors. However, the QLIF neuron suffers from important limitations. First, each QLIF neuron is essentially a classical LIF unit emulated on a single qubit, which restricts it to limited, classical-like state dynamics. Second, the QLIF neuron requires multi-shot measurements to determine spike events. The neuron’s spiking behavior is determined by thresholding the excitation probability of one qubit, and deciding whether to fire requires estimating this probability via repeated quantum measurements at each time step. This multi-shot scheme incurs significant overhead, as the quantum state must be prepared and measured many times to obtain one spike decision. Third, training QLIF networks has so far relied on classical backpropagation through time on a classical simulator. This global, offline learning approach makes it

challenging to deploy or adapt the model directly on quantum hardware for online learning.

Overall, existing hybrid models like QRC and QLIF validate the concept of quantum neuromorphic systems, but they either treat the quantum device as a black-box dynamical system or implement spiking neurons in a way that closely resembles classical models. There is a clear need for new designs that fully exploit quantum dynamics while supporting efficient operation and learning on hardware.

In this work, we address this knowledge gap by proposing the stochastic quantum spiking (SQS) neuron and corresponding SQS neural networks (SQSNNs). In contrast to QLIF, as illustrated in Fig. 1, each SQS neuron is realized with a multi-qubit quantum circuit, endowing the neuron with an internal quantum memory and richer dynamics (see Fig. 1(a)). SQS neurons produce spikes in an event-driven, single-shot manner, requiring no repeated measurements, while networks of SQS neurons (see Fig. 1(b)) can be trained using a hardware-compatible local learning rule (see Fig. 1(c)).

Main Contributions

The main features of the proposed SQS neuron and SQSNN architecture are as follows:

- **Multi-qubit neuron with quantum memory:** Each SQS neuron is implemented as a multi-qubit quantum circuit, allowing it to exploit entangled states and richer internal dynamics. This design increases the expressive capacity of each neuron and ensures the model fully leverages quantum hardware. Specifically, the SQS neuron employs an internal quantum memory mechanism inspired by quantum recurrent neural networks (QRNNs)^{18–20}, so that the neuron’s multi-qubit state carries quantum information from one time step to the next, preserving a trace of its previous inputs and activity.
- **Event-driven, single-shot spiking:** SQS neurons generate output spikes probabilistically in an event-driven manner based on a single-shot measurement of the multi-qubit state. In contrast to QLIF’s multi-shot probability estimation, an SQS neuron emits spikes within one quantum evolution, with spike events occurring stochastically (according to Born’s rule). This aligns with the neuromorphic principle that computations must be driven by input events, while avoiding costly repeated measurements.
- **Hardware-compatible local learning:** We develop a learning rule for SQSNNs that updates synaptic weights using only information locally available at each neuron, avoiding global backpropagation on a classical simulator. This bio-inspired scheme runs natively on quantum hardware, adjusting connection strengths based on stochastic spike coincidences, akin to three-factor learning rules in neuromorphic computing^{21,22}.

Overall, the SQS model harnesses quantum resources—multiple qubits, entanglement, inherent randomness—to implement a spiking neuron that operates in an event-driven probabilistic manner akin to well-studied models of biological neurons²³. The architecture is particularly suited for quantum hardware with (i) low repetition rate—i.e., systems with high shot-to-shot latency such as trapped-ion or neutral-atom platforms²⁴, and (ii) support for mid-circuit measurements, which are needed

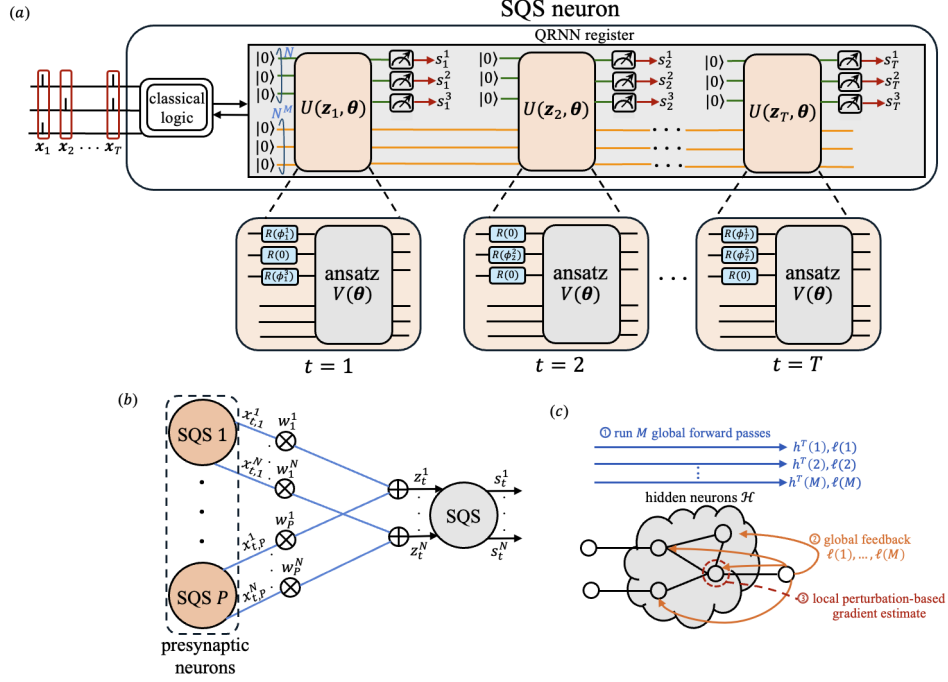


Fig. 1 (a) Stochastic quantum spiking (SQS) neuron model. Schematic of an SQS neuron with $N^I = 3$ input-output qubits (green) and $N^M = 3$ memory qubits (orange), receiving input from P presynaptic neurons. At each time t , incoming presynaptic spikes are summed (blue arrows) into input currents $\mathbf{z}_t = [z_t^1, \dots, z_t^N]$. The currents determine rotation angles ϕ_t applied to the input qubits (blue gates). A parameterized quantum circuit (PQC, gray box) with trainable parameters θ entangles input and memory qubits, updating the neuron's state. The N input qubits are then measured (meter symbols) to produce output spikes s_t (red arrows), after which those qubits are reset to the nominal state $|0\rangle$. The memory qubits are not measured, preserving quantum information (orange shading) that influences subsequent time steps. This internal quantum memory allows the SQS neuron to exhibit complex temporal dynamics, while not requiring multi-shot measurements. **(b) Synaptic connections in an SQS neural network (SQSNN).** The n -th input current z_t^n of the SQS neuron is computed as the weighted sum of the corresponding spiking signal $\{x_{t,p}^n\}_{p=1}^P$ from the P presynaptic neurons. **(c) Local zeroth-order learning rule.** At each iteration, the proposed local zeroth-order learning rule implements: ① M global forward passes, where M is a constant M independent of the number of parameters, ② the evaluation of M global feedback signals at the output SQS neurons, and ③ local perturbation-based, zeroth-order updates within each neuron.

to realize the QRNN-based quantum memory mechanism. Mid-circuit measurements are available in several superconducting qubit systems, and they are also emerging in trapped-ion and atom platforms^{25,26}. Due to their reliance on mid-circuit measurements, SQSNNs can be viewed as examples of dynamic parameterized quantum circuits (PQCs), which have been recently shown to have significant advantages in terms of expressivity and trainability.²⁷

Results

SQS neuron architecture

An SQS neuron extends classical probabilistic spiking neurons by utilizing a multi-qubit register as an internal (quantum) state memory, along with a measurement-based single-shot spike generation mechanism. As illustrated in Fig. 1(a), each SQS neuron comprises N^{tot} qubits split into two groups: N input-output qubits and N^{M} memory qubits, with $N^{\text{tot}} = N + N^{\text{M}}$.

At each discrete time t , a single-shot measurement of the input-output qubits produces N binary signals to be propagated to downstream neurons—with values 0 and 1 corresponding to the absence or presence of a spike, respectively. The input-output qubits are then reset to the nominal state $|0\rangle$ at the start of the next discrete time. The number N of input-output signals determines the number of (interacting) channels simultaneously processed by an SQS neuron.

Unlike the input-output qubits, the memory qubits carry quantum information forward across time without being measured. Thus, each SQS neuron retains a hidden state in the memory qubits, playing the role of the membrane potential in classical spiking models.

As shown in Fig. 1(b), with an SQSNN, the operation of each SQS neuron is driven by spikes received from a set of P presynaptic neurons. Let $\mathbf{x}_{t,p} \in \{0, 1\}^N$ be the binary outputs of presynaptic neuron p at time t , for $p = 1, \dots, P$. These inputs are first converted into an N -dimensional input current vector $\mathbf{z}_t = [z_t^1, \dots, z_t^N]$ by a classical mixed-signal CMOS logic circuit. This mechanism is identical to how inputs are aggregated in a classical spiking neuron²³. Specifically, for each output index n , the input current z_t^n is computed as a weighted sum of the corresponding presynaptic spikes

$$z_t^n = \sum_{p=1}^P w_p^n x_{t,p}^n, \quad (1)$$

where w_p^n is the synaptic weight from neuron p 's n -th output to this neuron's n -th input. Accordingly, the cost of this computation scales with the number of presynaptic spikes rather than with the number P of the presynaptic neurons, demonstrating the expected event-driven behavior of neuromorphic systems.

Each input current z_t^n is embedded into the state of the n -th input-output qubit. In particular, for each channel n , if the current z_t^n is positive, i.e., $z_t^n > 0$, a single-qubit rotation $R_X(\phi_t^n)$ is applied to the n -th input-output qubit with angle $\phi_t^n = \pi z_t^n$. Otherwise, if the current z_t^n is non-positive, i.e., $z_t^n \leq 0$, no rotation is applied. This way, when the current is non-positive, the corresponding n -th input-output qubit remains in the nominal state $|0\rangle$, requiring no rotation to be applied to it. Through this mechanism, sparse inputs, resulting in zero currents, naturally reduce not only the complexity of the classical logic but also the need for internal quantum operations.

After the input currents are embedded into the states of the input-output neurons, following the QRNN ansatz^{18–20}, a PQC $V(\boldsymbol{\theta})$ acts on the combined $(N + N^{\text{M}})$ -qubit register. This PQC entangles the input and memory qubits and evolves the state according to trainable parameters $\boldsymbol{\theta}$. For example, a simple choice (used in our

experiments) is to apply a layer of controlled rotations from each input qubit to each memory qubit, followed by single-qubit rotations on all qubits.

After this quantum processing step, the N input-output qubits are measured in the computational basis, yielding a binary outcome $s_t^n \in \{0, 1\}$ for each qubit n . These measurements produce the neuron’s output spikes $\mathbf{s}_t = [s_t^1, \dots, s_t^N]$ across the N channels. The memory qubits are not measured, and thus retain quantum state information, carrying it into time $t + 1$.

As discussed, spike generation in the SQS neuron is stochastic, occurring within a single shot via mid-circuit measurements. By Born’s rule, the probability of the neuron producing a particular N -bit spike pattern \mathbf{s}_t at time t is

$$p(\mathbf{s}_t) = \langle \mathbf{s}_t | \rho_t^I | \mathbf{s}_t \rangle, \quad (2)$$

where ρ_t^I is the reduced density matrix of the N input qubits prior to measurement. Given that the reduced density matrix ρ_t^I is affected by the interactions with the memory qubits via the PQC $V(\boldsymbol{\theta})$, the distribution (2) of the spiking outputs establishes a probabilistic mapping from the history of presynaptic and own past spikes to new output spikes, with the quantum memory enabling dynamics beyond classical integrate-and-fire.

Hardware-friendly local learning rule

As we demonstrate next, a key advantage of networks of SQS neurons—or SQSNNs—is the potential to train the network in situ on quantum hardware via a learning rule that borrows the key principles of locality and global feedback from classical neuromorphic computing^{21,22}.

The goal of learning is to optimize the parameters of each neuron, namely the synaptic weights \mathbf{w} used in the evaluation of the current (1) and the somatic PQC gate angles $\boldsymbol{\theta}$. The proposed learning method is local in the sense that each neuron adjusts its parameters using only information resulting from its own activity, along with scalar feedback signals broadcast from the output layer of the network. This approach eliminates any need to compute gradients via global backpropagation through a classical simulator of the network, as done for QLIF networks¹³, or via global perturbation-based rules⁶.

During training, the SQSNN performs multiple quantum measurements per time step to estimate gradients using local perturbations. However, during inference, the network operates in a fully single-shot regime, generating one spike sample per neuron per time step based on the current quantum state without repeated measurements.

To elaborate, consider a supervised learning setting with a dataset of input–output examples consisting of spike sequences of duration T time steps. For any given input example in the data set, the SQSNN produces a stochastic output spiking sequence through its neurons in the output layer. For a well-trained SQSNN, the produced sequence must be likely to match the corresponding output spike sequence \mathbf{o}^T in the dataset. The match between actual and target output sequences is measured by the standard negative log-likelihood of the target output sequence, denoted as $\mathcal{L}_{\mathbf{o}^T}(\boldsymbol{\Theta})$.

Learning seeks to adjust all neuron parameters Θ —synaptic and somatic—to minimize the empirical average loss over the dataset via gradient descent. While computing the gradients of the exact loss is generally intractable due to the probabilistic recurrent coupling of neurons, a suitable bound $L_{\mathbf{o}^T}(\Theta)$ on the log-likelihood $\mathcal{L}_{\mathbf{o}^T}(\Theta)$, satisfying the inequality $L_{\mathbf{o}^T}(\Theta) \geq \mathcal{L}_{\mathbf{o}^T}(\Theta)$, can be derived that admits gradients with efficient estimates. The resulting gradient-based learning rule, illustrated in Fig. 1(c), requires each neuron to update its parameters through the product of a local gradient and of a global error feedback derived from the output loss. The following steps are applied at each learning iteration.

① **Global forward passes:** The SQSNN first runs M independent global forward passes through the network. During this phase, each neuron stores the corresponding local presynaptic spiking inputs.

② **Evaluation of global feedback signals:** Given the target output signals \mathbf{o}^T and using the results of the M forward passes, the output neurons of the SQSNN evaluate the M global feedback signals $\ell(1), \dots, \ell(M)$. These serve as an estimate of the bound $L_{\mathbf{o}^T}(\Theta)$ of the negative log-likelihood attainable with the current network parameters Θ .

③ **Local perturbation-based, zeroth-order updates within each neuron:** Each neuron i evaluates a local gradient using zeroth-order optimization methods for both synaptic weights $w_{i,j}$ and circuit angles $\theta_{i,k}$. Specifically, to adjust the synaptic weight vector \mathbf{w}_i , the neuron generates M_{syn} random perturbation vectors $\{\Delta \mathbf{w}_{i,m}\}_{m=1}^{M_{\text{syn}}}$ with components sampled independently from the Rademacher distribution. The weights are perturbed by small amounts $\epsilon \Delta \mathbf{w}_{i,m}$ for some small constant $\epsilon > 0$ in the positive and negative directions. The neuron i then observes the resulting change in its local spiking probability $p(\mathbf{s}_{i,t})$ via two M_p -shot measurements. Following simultaneous perturbation stochastic approximation (SPSA)²⁸, we average the results to obtain an estimate of the gradient $\nabla_{\mathbf{w}_i} \log p(\mathbf{s}_{i,t})$ (see Methods).

For each PQC angle $\theta_{i,k}$, neuron i uses the parameter-shift rule²⁹ by adopting the perturbed somatic parameters $\theta_{i,k} \pm \pi/2$ and computing the difference in output probabilities across $2M_{\text{som}}$ shots, estimating the partial derivative $\partial \log p(\mathbf{s}_{i,t}) / \partial \theta_{i,k}$.

The local gradient estimates are finally multiplied by the scalar feedback signals and accumulated over time to update the parameters. Pseudocode for the training procedure is provided in Algorithm 1 (see Methods).

Experiments

Tasks

In this section, we compare the performance of classical and quantum models—conventional and spiking—on standard datasets, such as MNIST, FMNIST and KMNIST as done in prior work¹³, as well as on neuromorphic datasets captured via event-driven cameras³⁰.

USPS binary classification: We first consider a simple binary classification task obtained from the USPS handwritten digit dataset by focusing on the digits “1” and “7”.²² Each input image is encoded into the spiking domain using rate encoding³¹: for each pixel, a spike train of $T = 10$ time steps is generated by sampling from a Bernoulli

distribution with spiking probability proportional to the pixel’s intensity. The class labels $\{1, 7\}$ are also represented using rate encoding during training. Specifically, there are two output neurons, and the target signal \mathbf{o}^T for the two output neurons are such that the neuron associated with the correct class emits a spike at each time step.²²

MNIST, FMNIST, and KMNIST image classification: We also consider image classification tasks based on the standard MNIST, FMNIST, and KMNIST datasets. In order to highlight the capacity of different models to process event-driven data, we encode the input images for the MNIST, FMNIST and KMNIST datasets and their labels using rate encoding and decoding with $T = 5$ time steps.

Neuromorphic data classification: Finally, to showcase the sequence modeling capabilities of SQSNN on event-driven data, we study classification tasks based on a neuromorphic dataset, namely MNIST-DVS³². The MNIST-DVS dataset consists of labeled spiking signals recorded by a dynamic vision sensor (DVS) while it observes handwritten digits moving on a screen with a duration of $T = 80$ time steps.³³

Benchmarks

In the following experiments, we benchmark the proposed SQSNN model against the following alternative models:

- **Classical SNN:** Classical feedforward SNN model based on LIF neurons, trained using surrogate gradient descent with backpropagation.³¹
- **QLIF-SNN:** Feedforward neural network implementing QLIF neurons.¹³
- **Quantum neural network (QNN):** A quantum variational classifier with classical input and read-out layers.³⁴ For this model, the input is first encoded using a single classical neural layer, and then processed by a PQC using angle embedding and entangling gates. The outputs are measured and passed to a classical fully connected layer.

All models are configured to have approximately the same number of parameters. This is a conventional benchmarking setting in quantum machine learning, as the number of parameters directly relates to key model properties such as trainability, complexity, and expressivity³⁵.

Evaluating the local learning rule on quantum hardware

We start by evaluating the properties of the proposed local learning rule, focusing on its per-iteration requirements in terms of the number of global forward passes, M , and the numbers of local shots at each neuron, namely $2M_{\text{syn}}$ for the synaptic weights and $2M_{\text{som}}$ for each PQC parameter.

To this end, we implement the local training rule on the IBM quantum computer `ibm.brisbane` using Qiskit.³⁶ In Fig. 2(a) and Fig. 2(b), we report the test accuracy of the SQSNN on the USPS dataset as a function of the training iterations, while varying the parameters M and M_{syn} with $M_{\text{som}} = 1$ and $M_p = 5$. Fig. 2(a) does not assume quantum error mitigation (QEM), while Fig. 2(b) implements QEM using the zero noise extrapolation algorithm provided by the Mitq library³⁶.

With $M = 1$ and $M_{\text{syn}} = 5$, the SQSNN model is seen to achieve a peak test accuracy of nearly 95%, even in the absence of QEM. In contrast, configurations

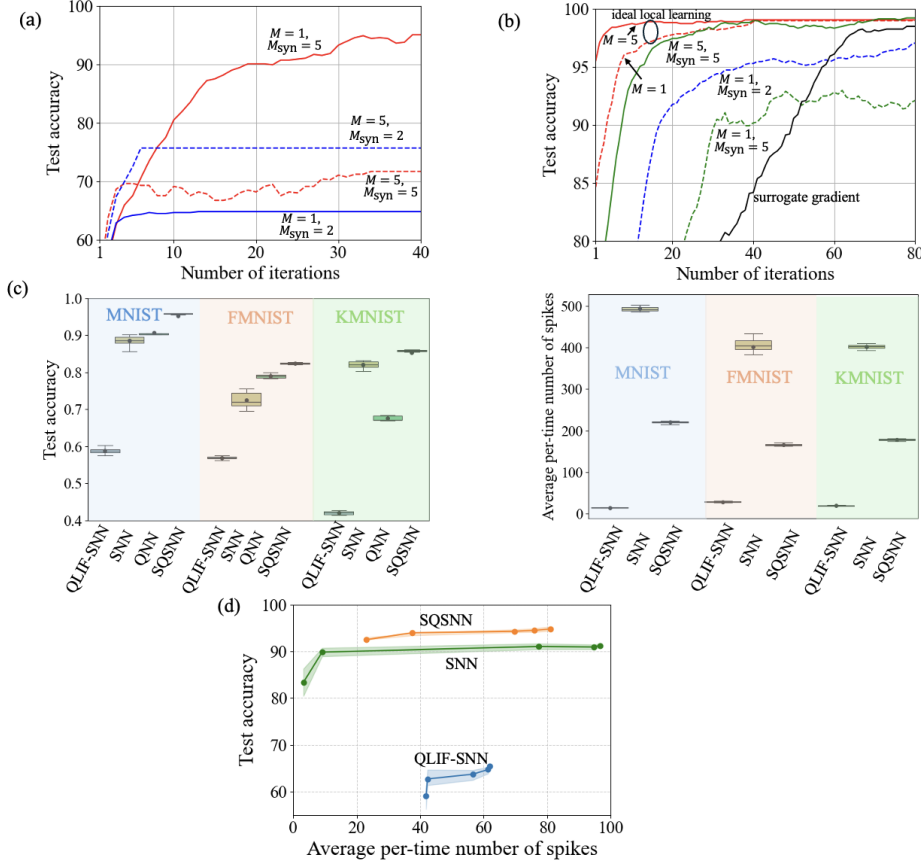


Fig. 2 (a) **Test accuracy versus training iterations on a NISQ device without QEM:** Test accuracy as a function of training iterations for the SQSNN model on the USPS dataset under the proposed local learning rule implemented on IBM’s `ibm_brisbane` without QEM. We vary the number of global passes M and measurement shots for synaptic weights M_{syn} , with $M_{\text{som}} = 1$. (b) **Test accuracy versus training iterations on a NISQ device with QEM:** Test accuracy as a function of training iterations for the SQSNN model on the USPS dataset under the proposed local learning rule, implemented on IBM’s `ibm_brisbane` with zero noise extrapolation algorithm. The ideal local learning refers to the proposed local learning rule with a perfect estimation of spiking probability (6), while the surrogate gradient method is an efficient approximate training approach based on classical simulations that is described in Supplementary Information. (c) **Test accuracy and average number of spike per time step on the MNIST, FMNIST, and KMNIST datasets:** The left panel shows box plots of test accuracy achieved by each model across ten runs on the three datasets, while the right panel shows the corresponding box plots for the average number of spikes per time step during inference. (d) **Accuracy versus average number of spikes per time step on the MNIST-DVS:** Neuromorphic dataset under varying regularization strengths λ in (3).

with lower shot counts for the synaptic weights, e.g., $M_{\text{syn}} = 2$, or a higher numbers of global forward passes, e.g., $M = 5$, exhibit reduced accuracy. The latter result suggests that increasing the number of forward passes may cause a higher susceptibility to decoherence and gate errors without QEM. Furthermore, increasing the number of measurement shots from $M_{\text{syn}} = 2$ to $M_{\text{syn}} = 5$ at fixed $M = 5$ yields only

a marginal improvement. Overall, the strong performance of the configuration with $(M = 1, M_{\text{syn}} = 5, M_{\text{som}} = 1)$ highlights the potential of local learning in hybrid quantum-classical systems, even with current NISQ devices without QEM.

Using the same hardware, Fig. 2(b) plots the test accuracy obtained by the SQSNN model on the USPS dataset as a function of training iterations with QEM. We set $M_{\text{som}} = 1$, and report results for the configurations $(M = 1, M_{\text{syn}} = 1)$, $(M = 1, M_{\text{syn}} = 2)$ and $(M = 5, M_{\text{syn}} = 5)$. For reference, we include the performance of an ideal local training algorithm in which the local gradients (24)-(25) are computed exactly. In practice, this would require either a classical model of the neuron or the use of a large number of shots M_{syn} and M_{som} . We also evaluate a surrogate gradient-based method inspired by methods for classical SNNs³¹, in which the spiking probability in (6) is replaced with a suitable sigmoid function, enabling the use of backpropagation. This scheme requires a classical simulator, providing a more efficient alternative for implementation on classical processor such as GPUs. We provide a brief description of this approach in Supplementary Information.

We observe from Fig. 2(b) that increasing either the number of global forward passes M or the number of measurement shots M_{syn} leads to improved test accuracy. However, it is generally necessary to increase both numbers in order to obtain the best performance. In particular, with $M = 5$ and $M_{\text{syn}} = 5$, SQSNN obtains a test accuracy around 98% at around 40 iterations, which matches that of the corresponding ideal local learning rule. Overall, the use of QEM is concluded to further improve the performance of SQSNNs, while also stabilizing its performance as a function of the number of global forward passes and shots.

Finally, the surrogate gradient-based strategy—which relies on an efficient classical simulation of the system—provides a close approximation of the performance of the ideal local learning rule at convergence. Based on these insights, in order to scale the evaluation to larger tasks and models, henceforth we use the surrogate gradient-based approach and rely on a classical simulator for all models.

Natural image classification tasks

We now present a comparative evaluation of the four models, SNN, QNN, QLIF-SNN and SQSNN, on the MNIST, FMNIST, and KMNIST image classification tasks. As shown in the left panel of Fig. 2(c), the SQSNN model consistently achieves the highest test accuracy across all three datasets, demonstrating its superior capacity to extract relevant features from input sequences. The box plots further indicate that SQSNN maintains this performance with low variability across runs. The classical SNN model also performs well, but lags behind the SQSNN, while the QNN and QLIF-SNN show comparatively lower accuracy, particularly on the more challenging KMNIST dataset.

Following common practice in neuromorphic engineering³⁷, we also report the average number of spikes per time step during inference. This quantity represents the aggregate spike count across the entire network, rather than per-neuron spiking activity. We adopt this measure to fairly compare models that differ in neuron count, but are constrained to a similar total parameter budget. As discussed earlier, the number of spikes provides a useful measure of the classical and quantum processing complexity of the SQSNN. As seen in the right panel of Fig. 2(c), the QLIF-SNN model

exhibits the lowest number of spikes, but at the cost of a substantially lower accuracy. Notably, the SQSNN model achieves the most favorable performance trade-off, maintaining both high accuracy and moderate spiking activity. This balance highlights the potential of the SQSNN for energy-efficient neuromorphic computing, especially in hardware-constrained environment. For reference, the per-neuron spike statistics for each model are provided in the Supplementary Information.

Neuromorphic vision classification task

We now evaluate all spiking models—SNN, QLIF-SNN, and SQSNN—on the MNIST-DVS dataset³². In order to explore the trade-off between accuracy and number of spikes, we add to the training objective (16) the regularization term

$$\frac{\lambda}{T} \sum_{t=1}^T \frac{(\sum_i u_{i,t})^2}{\sum_i |u_{i,t}|^2}, \quad (3)$$

where $u_{i,t}$ is a measure related to the spiking rate of neuron i at time t , $\lambda > 0$ is a hyperparameter, and the sum over index i is evaluated separately for each layer. Specifically, for the SQSNN, the quantity $u_{i,t}$ denotes the spiking probability $p(s_{i,t} = 1)$; for the QLIF-SNN, it represents the spiking probability given by multi-shot measurements¹³; and for the classical SNN, it corresponds to the membrane potential³¹. The regularizer (3) promotes the sparsity of the vector with entries $\{u_{i,t}\}_i$, encouraging lower spiking rates.

In Fig. 2(d), we compare the test accuracy versus the average number of spikes per time step for the SNN, QLIF-SNN, and SQSNN models on the MNIST-DVS dataset under different regularization strengths λ . The results demonstrate that the SQSNN consistently outperforms both baseline models, achieving the highest accuracy across a broad range of spiking sparsity levels. Notably, the SQSNN maintains high performance even with relatively few spikes, indicating its superior efficiency in processing spatio-temporal event-based data. In contrast, the QLIF-SNN exhibits significantly lower accuracy at similar or higher spike counts. This highlights the effectiveness of the quantum-enhanced architecture of SQSNN in extracting discriminative features from neuromorphic inputs.

Discussion

We introduced a stochastic quantum spiking (SQS) neuron model, demonstrating that it enables SQS neural networks (SQSNNs) that combine quantum computing and neuromorphic design. The SQS neuron leverages a multi-qubit quantum state to provide inherent memory and single-shot, event-driven spike generation, avoiding the repeated measurements and classical memory used in prior quantum spiking models¹³. We further proved that SQSNNs can be trained using a local, hardware-efficient learning rule that relies only on perturbation-based estimates and scalar global feedback signals, with no global backpropagation or global zeroth-order gradient estimates.

Our results indicate that SQSNNs can achieve competitive or superior accuracy compared to both classical SNNs and previous quantum neural models, while operating

at potentially lower spiking rates. This may be attributed to the SQS neuron’s hybrid architecture, which combines quantum memory with stochastic spiking, enabling richer temporal dynamics without requiring resets or repeated measurements. This architecture allows the model to capture more expressive input-output mappings while maintaining sparse activity. In contrast, the QLIF-SNN exhibits low spike counts due to its leaky integration mechanism and multi-shot measurement scheme, which heavily suppresses spike generation. While this leads to an energy-efficient operation, it also severely limits the neuron’s expressivity, contributing to its significantly lower accuracy. This suggests that quantum enhancements—expanded state space and inherent stochasticity—can be harnessed to improve learning and efficiency in neuromorphic systems. SQSNNs thus represent a promising direction for hybrid quantum neuromorphic intelligence based on dynamic PQCs, offering a scalable path toward trainable quantum spiking networks on near-term hardware.

By marrying the sparse temporal processing of neuromorphic computing with the large state space of quantum computing, SQSNNs point toward a new class of AI models capable of learning and inference in regimes beyond the reach of traditional approaches. The persistent internal quantum memory states of SQS neurons may be particularly promising for capturing long-range dependencies and contextual information across time. Future work may explore combining SQS neurons with structured state-space models (SSMs) to further enhance temporal modeling capacity, alongside the integration with tailored quantum error mitigation strategies³⁸, while also addressing theoretical aspects around the expressivity and trainability²⁷ of SQSNNs.

Methods

SQS neuron quantum model

As illustrated in Fig. 1(a), an SQS neuron can process and produce N spikes, acting as a multiple-input multiple-output unit. The SQS neuron is composed of a classical logic module that encodes incoming data into quantum rotation gates, along with a QRNN module^{18,20} that plays the role of quantum memory.

At each discrete time $t = 1, \dots, T$, a PQC defined by a parameterized unitary transformation $U(\mathbf{z}_t, \boldsymbol{\theta})$ operates on the register of $N + N^M$ qubits, where $\boldsymbol{\theta}$ are parameters of the PQC to be optimized. Assuming that the neuron is connected to P pre-synaptic neurons, at each time t , the neuron processes NP incoming spiking signals $\mathbf{x}_t = [\mathbf{x}_{t,1}, \dots, \mathbf{x}_{t,P}]^T$ with $\mathbf{x}_{t,p} = [x_{t,p}^1, \dots, x_{t,p}^N]^T \in \{0, 1\}^N$ representing the N spiking signals produced by the p -th pre-synaptic neuron. The SQS neuron produces N spiking signals $\mathbf{s}_t = [s_t^1, \dots, s_t^N]^T \in \{0, 1\}^N$ by measuring the N input-output qubits through the following steps:

- **Quantum embedding:** Convert the $NP \times 1$ input signals \mathbf{x}_t into $N \times 1$ input currents $\mathbf{z}_t = [z_t^1, \dots, z_t^N]$ using (1), and embed the input currents \mathbf{z}_t into the state of the input-output qubits via rotation gates;
- **Quantum memory retrieval:** Following the QRNN model, jointly evolve input-output qubits and memory qubits;

- **Single-shot measurements:** Measure the N input-output qubits to produce the $N \times 1$ spiking signals \mathbf{s}_t .

At each time t , the input-output qubits are initialized to the ground state $|0\rangle^{\otimes N}$, and the rotation gates $\{R_X(\phi_t^n)\}_{n=1}^N$ are applied to embed the input currents \mathbf{z}_t . The input-output qubits, along with the memory qubits in the second group, are processed by a PQC defined by a unitary matrix $V(\boldsymbol{\theta})$. Accordingly, the overall unitary transformation $U(\mathbf{z}_t, \boldsymbol{\theta})$ applied by the SQS neuron to the initial state of the $(N + N^M)$ -qubit register can be expressed as

$$U(\mathbf{z}_t, \boldsymbol{\theta}) = V(\boldsymbol{\theta}) \cdot \left(\bigotimes_{n=1}^N R_X(\phi_t^n) \otimes I \right), \quad (4)$$

where I is a $2^{N^M} \times 2^{N^M}$ identity matrix and \otimes stands for the tensor product, which combines individual single-qubit operations into a joint operation over the full multi-qubit register.

After the joint transformation (4), the input-output qubits are measured to generate the output spiking signal $\mathbf{s}_t \in \{0, 1\}^N$. In contrast, the memory qubits are not measured, retaining information across time steps.

Denote as ρ_t^{IM} the density matrix of the $N + N^M$ qubits at the beginning of time interval t and as

$$\rho_t^{\text{I}} = \text{Tr}_{\text{M}}(\rho_t^{\text{IM}}), \quad (5)$$

the corresponding reduced density matrix for the input-output qubits. By Born's rule, the probability of producing the output signals $\mathbf{s}_t \in \{0, 1\}^N$ is given by

$$p(\mathbf{s}_t | \rho_t^{\text{I}}) = \langle \mathbf{s}_t | \rho_t^{\text{I}} | \mathbf{s}_t \rangle, \quad (6)$$

where $|\mathbf{s}_t\rangle = |s_t^1, \dots, s_t^N\rangle$.

Furthermore, as the input-output qubits collapse onto the computational state $|\mathbf{s}_t\rangle$, the post-measurement state of the memory qubits is described by the density matrix

$$\sigma_t^{\text{M}} = \frac{(\langle \mathbf{s}_t | \otimes I) \rho_t^{\text{IM}} (|\mathbf{s}_t\rangle \otimes I)}{\langle \mathbf{s}_t | \rho_t^{\text{I}} | \mathbf{s}_t \rangle}, \quad (7)$$

where I is a $2^{N^M} \times 2^{N^M}$ identity matrix. Accordingly, upon the application of the given unitary matrix (4), the density matrix of all the qubits at the following time step $t + 1$ is

$$\rho_{t+1}^{\text{IM}} = U(\mathbf{z}_t, \boldsymbol{\theta}) (|0\rangle\langle 0|^{\otimes N} \otimes \sigma_t^{\text{M}}) U(\mathbf{z}_t, \boldsymbol{\theta})^\dagger. \quad (8)$$

Through the relation (8), as anticipated, the state σ_t^{M} of the second group of qubits serves as quantum memory.

Finally, at the initial time $t = 1$, the N^{tot} qubits are all initialized to the ground state $|0\rangle$, so that the initial density matrix of the N^{tot} qubits is given by the separable state $\rho_0^{\text{IM}} = |0\rangle\langle 0|^{\otimes N} \otimes |0\rangle\langle 0|^{\otimes N^{\text{M}}}$. After processing of the first incoming current signal \mathbf{z}_1 via the unitary transformation (4), the resulting density matrix is $\rho_1^{\text{IM}} = U(\mathbf{z}_1, \boldsymbol{\theta})\rho_0^{\text{IM}}U(\mathbf{z}_1, \boldsymbol{\theta})^\dagger$.

Derivation of local learning rule

Similar to conventional neural models and to the QLIF neuron¹³, the proposed SQS neuron can be structured into a neural network that can be trained to perform specific tasks. In this section, we first describe a general network architecture based on SQS neurons, and then detail the learning rule introduced earlier. Technically, this result is obtained by leveraging the probabilistic, autoregressive, structure of the model induced by a network of SQS neurons.

SQS-based neural network model

As shown in Fig. 3, an SQSNN consists of a directed graph $(\mathcal{S}, \mathcal{E})$ encompassing a set \mathcal{S} of SQS neurons. The neurons are connected via directed edges described by a set $\mathcal{E} \subseteq \{(i, j) \text{ with } i, j \in \mathcal{S} \text{ and } i \neq j\}$ of ordered pairs (i, j) . Accordingly, each neuron i within the SQSNN receives inputs from a set \mathcal{P}_i of pre-synaptic neurons, with $\mathcal{P}_i = \{j \in \mathcal{S} : j \neq i \text{ and } (j, i) \in \mathcal{E}\}$. The number of pre-synaptic neurons for neuron i is thus $P_i = |\mathcal{P}_i|$.

Following the literature on neuromorphic systems^{22,39}, we partition the SQS neurons in the SQSNN into two disjoint subsets: the subset \mathcal{O} of output neurons and the subset \mathcal{H} of hidden neurons, with $\mathcal{S} = \mathcal{O} \cup \mathcal{H}$. The spiking signals of the output neurons provide the outputs of the SQSNN. In contrast, the spiking signals of the hidden neurons serve as internal representations guiding the output neurons towards producing informative signals.

Furthermore, as illustrated by the example in Fig. 3, the output neurons do not have any outgoing edges, representing the last layer of the network. Mathematically, we have the condition

$$\mathcal{P}_i \cap \mathcal{O} = \emptyset, \quad (9)$$

or equivalently $\mathcal{P}_i \cap \mathcal{H}_i = \mathcal{P}_i$, for all neurons $i \in \mathcal{S}$.

When the PQC's of all neurons are fixed and not trained, the SQSNN architecture introduced here can be interpreted as a form of quantum reservoir computing (QRC) with mid-circuit measurements^{16,17,40}. In it, the neurons serve as module of the reservoir with classical communication between modules, defined via mid-circuit measurements.

Probabilistic autoregressive model

At each time t , each (hidden or output) neuron i , receives the spiking signals $\mathbf{s}_{\mathcal{P}_i, t} \in \{0, 1\}^{N_{P_i}}$ from its pre-synaptic neurons in set \mathcal{P}_i , and produces a spiking vector-valued signal $\mathbf{s}_{i, t} \in \{0, 1\}^N$. Denote the past spiking output of any neuron $i \in \mathcal{S}$ up to time

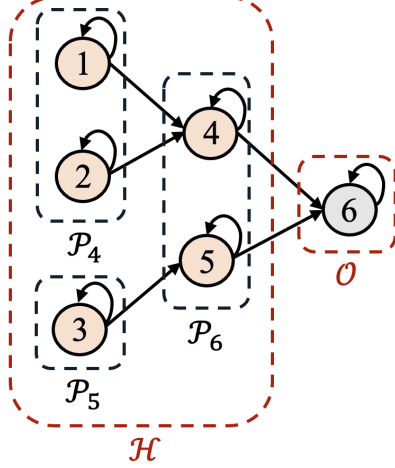


Fig. 3 Example SQS neural network (SQSNN). Directed graph of an SQSNN with six neurons ($S = \{1, \dots, 6\}$). Edges ($i \rightarrow j$) indicate neuron i feeds into neuron j . Neurons $\{1, 2, 3, 4, 5\}$ are hidden, and neuron 6 is the only output neuron ($\mathcal{O} = \{6\}$). Output neurons have no outgoing edges. Each node is an SQS neuron as in Fig. 1(a), with a self-loop denoting dependence on its own past spikes. The network's joint spike probability factorizes along these connections: e.g., neuron 6's spiking at time t depends only on the past spikes of neurons 4, 5 (its parents, denoted as \mathcal{P}_6) and on its own past spikes.

$t - 1$ as $\mathbf{s}_i^{t-1} = [\mathbf{s}_{i,1}, \dots, \mathbf{s}_{i,t-1}]$, and the collection of all past spiking outputs of any subset $S' \subseteq S$ of neurons as $\mathbf{s}_{S'}^{t-1} = \{\mathbf{s}_i^{t-1}\}_{i \in S'}$. Following the SQS model, the signal $\mathbf{s}_{i,t}$ produced by neuron i at any time t depends on the past spiking outputs $\mathbf{s}_{\mathcal{P}_i \cup \{i\}}^{t-1}$ from itself and from the pre-synaptic neurons \mathcal{P}_i .

Specifically, the dependence of the spiking history $\mathbf{s}_{\mathcal{P}_i \cup \{i\}}^{t-1}$ is reflected by the expression (6) of the spiking probability as a function of the neuron's state $\rho_{i,t}^I$ of the input-output qubits of neuron i . In fact, by the dynamic update (8), the state $\rho_{i,t}^I$ of the input-output qubits of neuron i evolves as a function of the sequence $\mathbf{s}_{\mathcal{P}_i \cup \{i\}}^{t-1}$ through the currents (1). Accordingly, the spiking probability of neuron i at time t , when conditioned on the sequence $\mathbf{s}_{\mathcal{P}_i \cup \{i\}}^{t-1}$, can be written using (6) as

$$p_{\Theta_i}(\mathbf{s}_{i,t} | \mathbf{s}_{\mathcal{P}_i \cup \{i\}}^{t-1}) = \langle \mathbf{s}_{i,t} | \rho_{i,t}^I | \mathbf{s}_{i,t} \rangle. \quad (10)$$

The notation $p_{\Theta_i}(\mathbf{s}_{i,t} | \mathbf{s}_{\mathcal{P}_i \cup \{i\}}^{t-1})$ emphasizes the dependence of the probability (10) on the local parameters $\Theta_i = \{\mathbf{w}_i, \boldsymbol{\theta}_i\}$ of neuron i . These include the synaptic weights $\mathbf{w}_i = \{\{w_{i,p}^n\}_{p=1}^{P_i}\}_{n=1}^N$ between the N input-output qubits of the P_i pre-synaptic neurons and the corresponding N qubits of neuron i , as well as the parameters $\boldsymbol{\theta}_i$ of the PQC in neuron i . Indeed, the state $\rho_{i,t}^I$ is obtained via (5) and (8), where the unitary transformation $U(\mathbf{z}_{i,t}, \boldsymbol{\theta}_i)$ in (4) depends on the variational parameters $\boldsymbol{\theta}_i$.

Denote as $\Theta = \{\Theta_i\}_{i \in S}$ the collection of all model parameters. By applying the chain rule, the joint spiking probability $\mathbf{s}^t = [\mathbf{s}_1^t, \dots, \mathbf{s}_{|S|}^t]$ of all neurons in the SQSNN

up to time T can be factorized over time index t and over neuron i as

$$\begin{aligned} p_{\Theta}(\mathbf{s}^T) &= \prod_{t=1}^T p_{\Theta}(\mathbf{s}_t | \mathbf{s}^{t-1}) \\ &= \prod_{t=1}^T \prod_{i \in \mathcal{S}} p_{\Theta_i}(\mathbf{s}_{i,t} | \mathbf{s}_{\mathcal{P}_i \cup \{i\}}^{t-1}). \end{aligned} \quad (11)$$

This corresponds to a probabilistic autoregressive sequence model akin to probabilistic spiking models studied in prior art^{22,39}.

Denote the spiking signals emitted by the output neurons as $\mathbf{o}_t = \{\mathbf{o}_{i,t}\}_{i \in \mathcal{O}}$, with $\mathbf{o}_{i,t} = [o_{i,t}^1, \dots, o_{i,t}^N]$, while the spiking signals emitted by the hidden neurons are written as $\mathbf{h}_t = \{\mathbf{h}_{i,t}\}_{i \in \mathcal{H}}$, with $\mathbf{h}_{i,t} = [h_{i,t}^1, \dots, h_{i,t}^N]$. As mentioned, the signals \mathbf{o}_t correspond to the model output (see Fig. 3). We also denote as $\Theta^{\mathcal{O}} = \{\Theta_i\}_{i \in \mathcal{O}}$ and $\Theta^{\mathcal{H}} = \{\Theta_i\}_{i \in \mathcal{H}}$ the sets of local parameters for the observed and hidden neurons, respectively. With these definitions, given that, by (9), the output neurons have no outgoing edges, the probability (11) can be expressed as

$$p_{\Theta}(\mathbf{s}^T) = \prod_{t=1}^T p_{\Theta^{\mathcal{H}}}(\mathbf{h}_t | \mathbf{h}^{t-1}) p_{\Theta^{\mathcal{O}}}(\mathbf{o}_t | \mathbf{o}^{t-1}, \mathbf{h}^{t-1}), \quad (12)$$

where the spiking probability $p_{\Theta^{\mathcal{H}}}(\mathbf{h}_t | \mathbf{h}^{t-1})$ of the hidden neurons does not depend on the spiking probability of the output neurons due to the assumption (9).

Maximum likelihood learning

To train an SQSNN, we assume the availability of a dataset $\mathcal{D} = \{\mathbf{o}^T\}$ of sequences $\mathbf{o}^T = [\mathbf{o}_1, \dots, \mathbf{o}_T]$, where each sequence \mathbf{o}^T corresponds to an example of desired behavior for the output neurons. Note that the sequence \mathbf{o}^T in the training dataset is used to supervise the spiking activity of the output neurons $i \in \mathcal{O}$, while the spiking behavior of the hidden neurons is left unspecified by the data. In practice, the data typically also specifies the (classical) inputs to a number of neurons.^{22,39} The inclusion of inputs is not made explicit in set \mathcal{D} to simplify the notation.

By the standard *maximum likelihood* (ML) criterion, we aim at minimizing the empirical average log-loss on data set \mathcal{D} , yielding the optimized model parameters

$$\Theta^* = \arg \min_{\Theta} \left\{ \mathcal{L}_{\mathcal{D}}(\Theta) = \sum_{\mathbf{o}^T \in \mathcal{D}} \mathcal{L}_{\mathbf{o}^T}(\Theta) \right\}, \quad (13)$$

with the per-data-point log-loss

$$\begin{aligned} \mathcal{L}_{\mathbf{o}^T}(\Theta) &= -\log p_{\Theta}(\mathbf{o}^T) \\ &= -\log \sum_{\mathbf{h}^T} p_{\Theta}(\mathbf{s}^T), \end{aligned} \quad (14)$$

where $\sum_{\mathbf{h}^T}$ denotes the sum over all possible $2^{|\mathcal{H}|}$ values \mathbf{h}^T taken by the signals produced by hidden neurons. By (14), evaluating the log-loss $\mathcal{L}_{\mathbf{o}^T}(\Theta)$ requires marginalizing over the spiking signals of the hidden neurons.

A direct application of standard gradient-based methods in quantum machine learning to problem (13) is not feasible. In fact, this would require estimating the probabilities $p_{\Theta}(\mathbf{s}^T)$ in (14) for all possible realization \mathbf{h}^T of the hidden neurons. To address this problem, we proceed in two steps. First, we introduce a bound on the log-loss (14) that enables Monte Carlo estimation, removing the need for the exponential number of network runs required to evaluate the sum in (14). Second, using the bound, we derive a local learning rule based on local perturbation-based gradient estimates and a global scalar feedback signal.

Estimating a likelihood bound

To derive the proposed training method, we start by introducing an upper bound on the log-likelihood. Noting that the sum in (14) can be expressed as an expectation yields

$$\begin{aligned} \mathcal{L}_{\mathbf{o}^T}(\Theta) &= - \sum_{t=1}^T \log \mathbb{E}_{p_{\Theta H}(\mathbf{h}_t|\mathbf{h}^{t-1})} [p_{\Theta \mathcal{O}}(\mathbf{o}_t|\mathbf{o}^{t-1}, \mathbf{h}^{t-1})] \\ &\leq - \sum_{t=1}^T \mathbb{E}_{p_{\Theta H}(\mathbf{h}_t|\mathbf{h}^{t-1})} [\log p_{\Theta \mathcal{O}}(\mathbf{o}_t|\mathbf{o}^{t-1}, \mathbf{h}^{t-1})] \\ &= L_{\mathbf{o}^T}(\Theta), \end{aligned} \quad (15)$$

where the first equality comes from (12) and (14), while the second line follows from Jensen's inequality²². Based on (10) and (11), the upper bound $L_{\mathbf{o}^T}(\Theta)$ in (15) can be rewritten as

$$\begin{aligned} L_{\mathbf{o}^T}(\Theta) &= - \sum_{t=1}^T \sum_{i \in \mathcal{O}} \mathbb{E}_{p_{\Theta H}(\mathbf{h}_t|\mathbf{h}^{t-1})} [\log p_{\Theta \mathcal{O}_i}(\mathbf{o}_{i,t}|\mathbf{o}_{\mathcal{P}_i \cup \{i\}}^{t-1})] \\ &= - \sum_{t=1}^T \sum_{i \in \mathcal{O}} \mathbb{E}_{p_{\Theta H}(\mathbf{h}_t|\mathbf{h}^{t-1})} [\log (\text{Tr}(\rho_{i,t}^{\mathbf{I}} O_{i,t}))], \end{aligned} \quad (16)$$

where $\text{Tr}(\cdot)$ is the trace operation, and the observable $O_{i,t}$ is defined as

$$O_{i,t} = |\mathbf{o}_{i,t}\rangle\langle\mathbf{o}_{i,t}|. \quad (17)$$

The key advantages of the upper bound $L_{\mathbf{o}^T}(\Theta)$ in (16) is that it can be approximated via a Monte-Carlo estimate obtained by running forward passes on the model, with each forward pass producing random samples $\mathbf{h}_t \sim p_{\Theta H}(\mathbf{h}_t|\mathbf{h}^{t-1})$ for the spiking signals of the hidden neurons.

We are interested in minimizing the upper bound on the training loss $\mathcal{L}_{\mathcal{D}}(\Theta)$ in (13) given by $L_{\mathcal{D}}(\Theta) = \sum_{\sigma^T \in \mathcal{D}} L_{\sigma^T}(\Theta)$, i.e.,

$$\Theta^* = \arg \min_{\Theta} \left\{ L_{\mathcal{D}}(\Theta) = \sum_{\sigma^T \in \mathcal{D}} L_{\sigma^T}(\Theta) \right\}. \quad (18)$$

Local zeroth-order learning

Given the objective (18), a conventional-based scheme would estimate the gradient $\nabla_{\Theta} L_{\sigma^T}(\Theta)$ via local perturbations of *all* parameters.⁴¹ However, this would require a number of forward passes through the entire network that grows *linearly* with the number $|\Theta|$ of parameters in Θ .⁴¹ This becomes quickly impractical as the number of neurons grows. To address the computational and scalability challenges of conventional zeroth-order training, in this subsection, we propose a local learning rule that updates each neuron’s parameters using a constant number of global forward passes, irrespective of the number $|\Theta|$ of model parameters.

As illustrated in Fig. 1(c), given the current iterate Θ and a data point σ^T , we begin by running the SQSNN with parameters Θ for M forward passes to collect M samples $\mathbf{h}^T(1), \dots, \mathbf{h}^T(M)$ of the hidden spiking signals. After this initial phase, each neuron updates its local parameters using zeroth-order perturbation methods that require only local forward passes within each neuron. Finally, the model parameters are updated at each neuron based on the results of the local forward passes and the global feedback signals $\ell(1), \dots, \ell(M)$.

Accordingly, unlike conventional zeroth-order learning methods, which require a separate set of forward passes for each parameter^{6,7}, our method performs just one set of M forward runs, after which local updates are computed independently for each neuron.

To derive the local gradient updates within each neuron, we consider separately hidden and output neurons.

Output neurons: Using (16), the gradient with respect to the parameters $\Theta_i^{\mathcal{O}}$ of an output neuron $i \in \mathcal{O}$ is given by

$$\nabla_{\Theta_i^{\mathcal{O}}} L_{\sigma^T}(\Theta) = - \sum_{t=1}^T \mathbb{E}_{p_{\Theta^H}(\mathbf{h}_{\mathcal{P}_i, t} | \mathbf{h}_{\mathcal{P}_i}^{t-1})} \left[\nabla_{\Theta_i^{\mathcal{O}}} \log (\text{Tr}(\rho_{i,t}^{\text{I}} O_{i,t})) \right]. \quad (19)$$

This can be estimated by using the local hidden variables $\{\mathbf{h}_{\mathcal{P}_i}^T(m)\}_{m=1}^M$ extracted from the corresponding global realizations $\{\mathbf{h}^T(m)\}_{m=1}^M$ of the hidden neurons as

$$\hat{\nabla}_{\Theta_i^{\mathcal{O}}} L_{\sigma^T}(\Theta) = - \frac{1}{M} \sum_{m=1}^M \sum_{t=1}^T \nabla_{\Theta_i^{\mathcal{O}}} \log (\text{Tr}(\rho_{i,t}^{\text{I}}(m) O_{i,t}(m))), \quad (20)$$

where $\rho_{i,t}^{\text{I}}(m)$ is the density matrix of the input-output qubit of neuron i during the m -th local forward pass, and $O_{i,t}(m) = |\mathbf{o}_{i,t}(m)\rangle\langle \mathbf{o}_{i,t}(m)|$ is the corresponding m -th

observable. In this next subsection, we will discuss how to compute the local gradient $\nabla_{\Theta_i^{\mathcal{O}}} \log(\text{Tr}(\rho_{i,t}^{\text{I}}(m)O_{i,t}(m)))$

Hidden neurons: For any hidden neuron $i \in \mathcal{H}$, using the REINFORCE gradient²², the gradient with respect to the parameter $\Theta_i^{\mathcal{H}}$ is obtained as

$$\nabla_{\Theta_i^{\mathcal{H}}} L_{\sigma^T}(\Theta) = - \sum_{t=1}^T \mathbb{E}_{p_{\Theta^{\mathcal{H}}}(\mathbf{h}_t|\mathbf{h}^{t-1})} \left[\left(\sum_{i \in \mathcal{O}} \log \text{Tr}(\rho_{i,t}^{\text{I}} O_{i,t}) \right) \nabla_{\Theta_i^{\mathcal{H}}} \log(\text{Tr}(\rho_{i,t}^{\text{I}} H_{i,t})) \right], \quad (21)$$

where $H_{i,t} = |\mathbf{h}_{i,t}\rangle\langle\mathbf{h}_{i,t}|$ is the observable corresponding to the realization $\mathbf{h}_{i,t}$ of hidden neuron $i \in \mathcal{H}$. Define as

$$\ell_t(m) = - \sum_{i \in \mathcal{O}} \log \text{Tr}(\rho_{i,t}^{\text{I}}(m)O_{i,t}(m)) \quad (22)$$

the log-loss for the current data point σ^T evaluated using the m -th realization $\mathbf{h}^T(m)$ of the hidden neuron. As seen in Fig. 1(c), the quantities $\{\ell(1), \dots, \ell(M)\}$, with $\ell(m) = (\ell_1(m), \dots, \ell_T(m))$, are fed back to all hidden neurons at the end of time T , providing global feedback signals to all hidden neurons. Using this information, each neuron i estimates the gradient $\nabla_{\Theta_i^{\mathcal{H}}} L_{\sigma^T}(\Theta)$ as

$$\hat{\nabla}_{\Theta_i^{\mathcal{H}}} L_{\sigma^T}(\Theta) = \frac{1}{M} \sum_{m=1}^M \sum_{t=1}^T \ell_t(m) \nabla_{\Theta_i^{\mathcal{H}}} \log(\text{Tr}(\rho_{i,t}^{\text{I}}(m)H_{i,t}(m))). \quad (23)$$

Local gradient estimation

In this subsection, we focus on estimating the gradient $\nabla_{\Theta_i^{\mathcal{O}}} \log(\text{Tr}(\rho_{i,t}^{\text{I}}(m)O_{i,t}(m)))$ for any output neuron $i \in \mathcal{O}$ in (20) and the gradient $\nabla_{\Theta_i^{\mathcal{H}}} \log(\text{Tr}(\rho_{i,t}^{\text{I}}(m)H_{i,t}(m)))$ for any hidden neuron $i \in \mathcal{H}$ in (23). We write generically such gradients as $\nabla_{\Theta_i} \log(\text{Tr}(\rho_{i,t}^{\text{I}} S_{i,t}))$ with $S_{i,t} = |\mathbf{s}_{i,t}\rangle\langle\mathbf{s}_{i,t}|$. Recall that for each neuron $i \in \mathcal{S}$, the local parameters $\Theta_i = \{\mathbf{w}_i, \boldsymbol{\theta}_i\}$ include the synaptic weights \mathbf{w}_i and the PQC parameters $\boldsymbol{\theta}_i$. Therefore, estimating the gradient $\nabla_{\Theta_i} \log(\text{Tr}(\rho_{i,t}^{\text{I}} S_{i,t}))$ requires evaluating the gradients $\nabla_{\mathbf{w}_i} \log(\text{Tr}(\rho_{i,t}^{\text{I}} S_{i,t}))$ and $\nabla_{\boldsymbol{\theta}_i} \log(\text{Tr}(\rho_{i,t}^{\text{I}} S_{i,t}))$. These gradients depend on the realization $\mathbf{h}_{\mathcal{P}_i}^T$ of the signals of the parents \mathcal{P}_i of node i . As described next, we propose to estimate the former using simultaneous perturbation stochastic approximation (SPSA)²⁸, while the latter is estimated using the parameter shift rule (PSR). The use of the PSR for PQC parameters is standard, while SPSA can be more efficient than individual per-weight perturbations for synaptic weights.

Gradient with respect to the synaptic weights The synaptic weights $\mathbf{w}_i = \{\{w_{i,p}^n\}_{p=1}^{P_i}\}_{n=1}^N$ associated with each neuron i pertain to the NP_i links between the N input-output qubits of the P_i pre-synaptic neurons and the corresponding N qubits of neuron i . To estimate the gradient $\nabla_{\mathbf{w}_i} \log(\text{Tr}(\rho_{i,t}^{\text{I}} S_{i,t}))$ with respect to synaptic weight \mathbf{w}_i , we apply SPSA.

Algorithm 1 Local learning rule for SQS-based Neural Networks

Require: Training sequence \mathbf{o}^T extracted from dataset \mathcal{D}

Ensure: Learned model parameters Θ

- 1: **Initialize** parameters Θ
 - 2: **Feedforward sampling:**
 - 3: Collect M samples of the hidden spiking signals $\mathbf{h}^T(1), \dots, \mathbf{h}^T(M)$ and the corresponding global feedback signals $\ell(1), \dots, \ell(M)$ in (22)
 - 4: **Global feedback:**
 - 5: Broadcast global learning signals $\ell(1), \dots, \ell(M)$ to all hidden neurons
 - 6: **for** $t = 1$ to T **do**
 - 7: **Local gradient estimation:**
 - 8: **for** each neuron $i \in \mathcal{S}$ **do**
 - 9: Compute the gradient $\nabla_{\Theta_i} \log(\text{Tr}(\rho_{i,t}^I S_{i,t}))$ using (24) or (25)
 - 10: **end for**
 - 11: **end for**
 - 12: **Parameter update:**
 - 13: Compute the gradient for each neuron based on (20) or (23) and perform gradient descent
-

Accordingly, given the spiking signals of the parent neurons, neuron i runs a number of local forward passes to estimate the expected value $\text{Tr}(\rho_{i,t}^I S_{i,t})$ of the observable $S_{i,t}$ obtained with synaptic weights $\mathbf{w}_i + \epsilon \Delta \mathbf{w}_{i,m}$ and $\mathbf{w}_i - \epsilon \Delta \mathbf{w}_{i,m}$, where $\Delta \mathbf{w}_{i,m}$ is the m -th random perturbation vector with components drawn independently from the Rademacher distribution, and $\epsilon > 0$ represents the magnitude of the perturbation. We generate M_{syn} such independent perturbations $\{\Delta \mathbf{w}_{i,m}\}_{m=1}^{M_{\text{syn}}}$ for each neuron i . Denote as $\rho_{i,t}^I(\mathbf{w}_i + \epsilon \Delta \mathbf{w}_{i,m})$ and $\rho_{i,t}^I(\mathbf{w}_i - \epsilon \Delta \mathbf{w}_{i,m})$ the states of the input-output qubits with perturbed synaptic weights $\mathbf{w}_i + \epsilon \Delta \mathbf{w}_{i,m}$ and $\mathbf{w}_i - \epsilon \Delta \mathbf{w}_{i,m}$, respectively. To estimate the corresponding expectations $\text{Tr}(\rho_{i,t}^I(\mathbf{w}_i + \epsilon \Delta \mathbf{w}_{i,m}) S_{i,t})$ and $\text{Tr}(\rho_{i,t}^I(\mathbf{w}_i - \epsilon \Delta \mathbf{w}_{i,m}) S_{i,t})$, we apply M_p shots. Therefore, the number of local shots for each neuron i for the synaptic weights is $2M_p M_{\text{syn}}$. Writing as $\hat{O}_{i,m}^+$ and $\hat{O}_{i,m}^-$ the two estimates obtained with the m -th perturbation, the overall local gradient is estimated as

$$\hat{\nabla}_{\mathbf{w}_i} \log(\text{Tr}(\rho_{i,t}^I S_{i,t})) = \frac{1}{M_{\text{syn}}} \sum_{m=1}^{M_{\text{syn}}} \frac{\log \hat{O}_{i,m}^+ - \log \hat{O}_{i,m}^-}{2\epsilon} \Delta \mathbf{w}_{i,m}. \quad (24)$$

Gradient with respect to the PQC parameters To estimate the gradient $\nabla_{\theta_i} \log(\text{Tr}(\rho_{i,t}^I S_{i,t}))$ with respect to the PQC parameters θ_i , we apply the PSR to each individual PQC parameter $\theta_{i,j}$. Given the spiking signals from the parent neurons, neuron i performs a series of local forward passes to evaluate the expected value $\text{Tr}(\rho_{i,t}^I S_{i,t})$ using perturbed parameters $\theta_{i,j} + \pi/2$ and $\theta_{i,j} - \pi/2$. For each angle $\theta_{i,j}$, we generate M_{som} independent evaluations using these shifted values. Each expectation is estimated using M_p measurement shots per forward pass, leading to a total of $2M_p M_{\text{som}}$ local shots per angle $\theta_{i,j}$. Let $\hat{O}_{i,m}^+$ and $\hat{O}_{i,m}^-$ denote the measured estimates of the observable $S_{i,t}$ for the m -th perturbation with shifted parameters $\theta_{i,j} + \pi/2$ and

$\theta_{i,j} - \pi/2$, respectively. Using the chain rule and averaging over the M_{som} repetitions, the gradient is estimated as

$$\nabla_{\theta_{i,j}} \log (\text{Tr}(\rho_{i,t}^I S_{i,t})) = \frac{1}{\text{Tr}(\rho_{i,t}^I S_{i,t})} \cdot \frac{1}{M_{\text{som}}} \sum_{m=1}^{M_{\text{som}}} \frac{\hat{O}_{i,m}^+ - \hat{O}_{i,m}^-}{2}. \quad (25)$$

Experimental setup

For all tasks and models, we adopt fully-connected feedforward architectures. The output layers consists of as many neurons as there are classes. For spiking models, we use rate decoding, selecting the class whose corresponding neuron produces the largest number of spikes.

For the USPS dataset, we use fully connected models with a single, output, layer of two neurons. For the other datasets, the models also include a hidden layer. For the SQSNN, there are 1000 hidden neurons for the MNIST, FMNIST and KMNIST datasets, and 256 neurons for the MNIST-DVS dataset, while for the SNN and the QLIF-SNN baselines the number of hidden neurons is adjusted to match the total number of trainable parameters in the SQSNN. The QNN model is also set up to have the same number of parameters.

For each SQS neuron, we configure the quantum circuit with $N = 1$ input-output qubit and $N^M = 1$ memory qubit. The ansatz $U(\mathbf{z}, \boldsymbol{\theta})$ consists of a controlled-RX (CRX) gate followed by single-qubit RX rotations applied independently to each qubit, as in previous literature³⁴. The CRX gate is parameterized by a rotation angle θ , and is given by the unitary matrix

$$\text{CRX}(\theta) = \begin{bmatrix} 1 & 0 & 0 & 0 \\ 0 & 1 & 0 & 0 \\ 0 & 0 & \cos(\theta/2) & -i \sin(\theta/2) \\ 0 & 0 & -i \sin(\theta/2) & \cos(\theta/2) \end{bmatrix}.$$

Both the CRX and RX gates contain trainable parameters that are optimized during learning. Therefore, in this setting, each SQS neuron i has three parameters $\boldsymbol{\theta}_i$ to be learned.

Acknowledgements. This work was supported by the European Union’s Horizon Europe project CENTRIC (101096379), the Engineering and Physical Science Research Council (EPSRC) project (EP/X011852/1) and by Open Fellowships of the EPSRC (EP/W024101/1 and EP/X011356/1).

The authors are grateful to Andrea Gentile (Pasqal) for the useful feedback and advice on hardware implementation.

Author contributions. J.C. contributed to the conceptual development of the work, implemented the experimental models, performed analysis of the results and writing of the manuscript. B.R. provided inputs on the experimental validation, participated in the analysis of results, and contributed to writing the manuscript. O.S. conceived the research problem, designed the architectural and algorithmic framework,

led the experimental validation, writing of the manuscript, and overall supervision of the project.

References

- [1] Rajendran, B., Simeone, O., Al-Hashimi, B.M.: Towards efficient and trustworthy ai through hardware-algorithm-communication co-design. arXiv preprint arXiv:2309.15942 (2023)
- [2] Marković, D., Grollier, J.: Quantum neuromorphic computing. Applied physics letters **117**(15) (2020)
- [3] Nielsen, M.A., Chuang, I.L.: Quantum Computation and Quantum Information. Cambridge university press, Cambridge, UK (2010)
- [4] Mermin, N.D.: Quantum Computer Science: an Introduction. Cambridge University Press, Cambridge, UK (2007)
- [5] Simeone, O.: Classical and Quantum Uncertainty, Information, and Correlation. <https://sites.google.com/view/osvaldosimeone/cqit>. In preparation (2024)
- [6] Schuld, M., Petruccione, F.: Machine Learning with Quantum Computers vol. 676. Springer, Cham (2021)
- [7] Simeone, O., *et al.*: An introduction to quantum machine learning for engineers. Foundations and Trends® in Signal Processing **16**(1-2), 1–223 (2022)
- [8] Rajendran, B., Sebastian, A., Schmuker, M., Srinivasa, N., Eleftheriou, E.: Low-power neuromorphic hardware for signal processing applications: A review of architectural and system-level design approaches. IEEE Signal Processing Magazine **36**(6), 97–110 (2019)
- [9] Mehonic, A., Sebastian, A., Rajendran, B., Simeone, O., Vasilaki, E., Kenyon, A.J.: Memristors—from in-memory computing, deep learning acceleration, and spiking neural networks to the future of neuromorphic and bio-inspired computing. Advanced Intelligent Systems **2**(11), 2000085 (2020)
- [10] Davies, M., Wild, A., Orchard, G., Sandamirskaya, Y., Guerra, G.A.F., Joshi, P., Plank, P., Risbud, S.R.: Advancing neuromorphic computing with loihi: A survey of results and outlook. Proceedings of the IEEE **109**(5), 911–934 (2021)
- [11] Neftci, E.O., Mostafa, H., Zenke, F.: Surrogate gradient learning in spiking neural networks: Bringing the power of gradient-based optimization to spiking neural networks. IEEE Signal Processing Magazine **36**(6), 51–63 (2019) <https://doi.org/10.1109/MSP.2019.2931595>
- [12] Skatchkovsky, N., Jang, H., Simeone, O.: Bayesian continual learning via spiking

neural networks. *Frontiers in Computational Neuroscience* **Volume 16 - 2022** (2022)

- [13] Brand, D., Petruccione, F.: A quantum leaky integrate-and-fire spiking neuron and network. *npj Quantum Information* **10**(1), 1–8 (2024)
- [14] Dudas, J., Carles, B., Plouet, E., Mizrahi, F.A., Grollier, J., Marković, D.: Quantum reservoir computing implementation on coherently coupled quantum oscillators. *npj Quantum Information* **9**(1), 64 (2023)
- [15] Fujii, K., Nakajima, K.: Harnessing disordered-ensemble quantum dynamics for machine learning. *Physical Review Applied* **8**(2), 024030 (2017)
- [16] Lau, H.W., Hayashi, A., Sakurai, A., Munro, W.J., Nemoto, K.: Modular quantum extreme reservoir computing. *arXiv preprint arXiv:2412.19336* (2024)
- [17] Muraier, J., Krishnakumar, R., Tornow, S., Geierhos, M.: Feedback connections in quantum reservoir computing with mid-circuit measurements. *arXiv preprint arXiv:2503.22380* (2025)
- [18] Takaki, Y., Mitarai, K., Negoro, M., Fujii, K., Kitagawa, M.: Learning temporal data with a variational quantum recurrent neural network. *Physical Review A* **103**(5), 052414 (2021)
- [19] Bausch, J.: Recurrent quantum neural networks. In: Larochelle, H., Ranzato, M., Hadsell, R., Balcan, M.F., Lin, H. (eds.) *Advances in Neural Information Processing Systems*, vol. 33, pp. 1368–1379 (2020)
- [20] Nikoloska, I., Simeone, O., Banchi, L., Veličković, P.: Time-warping invariant quantum recurrent neural networks via quantum-classical adaptive gating. *Machine Learning: Science and Technology* **4**(4), 045038 (2023)
- [21] Frémaux, N., Gerstner, W.: Neuromodulated spike-timing-dependent plasticity, and theory of three-factor learning rules. *Frontiers in Neural Circuits* **Volume 9 - 2015** (2016)
- [22] Jang, H., Simeone, O., Gardner, B., Gruning, A.: An introduction to probabilistic spiking neural networks: Probabilistic models, learning rules, and applications. *IEEE Signal Processing Magazine* **36**(6), 64–77 (2019)
- [23] Gerstner, W., Kistler, W.M.: *Spiking Neuron Models: Single Neurons, Populations, Plasticity*. Cambridge University Press, Cambridge, UK (2002)
- [24] Gentile, A., Paesani, S., Santagati, R., Wang, J., Wiebe, N., Tew, D., O’Brien, J., Thompson, M.: Noise resilience of bayesian quantum phase estimation tested on a si quantum photonic chip. In: *European Quantum Electronics Conference*, pp. 6–2 (2017). Optica Publishing Group

- [25] Motlakunta, S., Kotibhaskar, N., Shih, C.-Y., Vogliano, A., McLaren, D., Hahn, L., Zhu, J., Hablützel, R., Islam, R.: Preserving a qubit during state-destroying operations on an adjacent qubit at a few micrometers distance. *Nature Communications* **15**(1), 6575 (2024)
- [26] Chen, Z.-Y., Goetting, I., Toh, G., Yu, Y., Shalaev, M., Saha, S., Kalakuntla, A., Shi, H.B., Monroe, C., Kozhanov, A., et al.: Non-invasive mid-circuit measurement and reset on atomic qubits. arXiv preprint arXiv:2504.12538 (2025)
- [27] Deshpande, A., Hinsche, M., Najafi, S., Sharma, K., Sweke, R., Zoufal, C.: Dynamic parameterized quantum circuits: expressive and barren-plateau free. arXiv preprint arXiv:2411.05760 (2024)
- [28] Spall, J.C.: An overview of the simultaneous perturbation method for efficient optimization. *Johns Hopkins apl technical digest* **19**(4), 482–492 (1998)
- [29] Wierichs, D., Izaac, J., Wang, C., Lin, C.Y.-Y.: General parameter-shift rules for quantum gradients. *Quantum* **6**, 677 (2022)
- [30] Gallego, G., et al.: Event-based vision: A survey. *IEEE transactions on pattern analysis and machine intelligence* **44**(1), 154–180 (2020)
- [31] Eshraghian, J.K., Ward, M., Neftci, E.O., Wang, X., Lenz, G., Dwivedi, G., Bennamoun, M., Jeong, D.S., Lu, W.D.: Training spiking neural networks using lessons from deep learning. *Proceedings of the IEEE* **111**(9), 1016–1054 (2023)
- [32] Serrano-Gotarredona, T., Linares-Barranco, B.: Poker-dvs and mnist-dvs. their history, how they were made, and other details. *Frontiers in neuroscience* **9**, 481 (2015)
- [33] Chen, J., Skatchkovsky, N., Simeone, O.: Neuromorphic wireless cognition: Event-driven semantic communications for remote inference. *IEEE Transactions on Cognitive Communications and Networking* **9**(2), 252–265 (2023)
- [34] Schuld, M., Bocharov, A., Svore, K.M., Wiebe, N.: Circuit-centric quantum classifiers. *Physical Review A* **101**(3), 032308 (2020)
- [35] Abbas, A., Sutter, D., Zoufal, C., Lucchi, A., Figalli, A., Woerner, S.: The power of quantum neural networks. *Nature Computational Science* **1**(6), 403–409 (2021)
- [36] Javadi-Abhari, A., Treinish, M., Krsulich, K., Wood, C.J., Lishman, J., Gacon, J., Martiel, S., Nation, P.D., Bishop, L.S., Cross, A.W., et al.: Quantum computing with qiskit. arXiv preprint arXiv:2405.08810 (2024)
- [37] Wu, D., Chen, J., Rajendran, B., Vincent Poor, H., Simeone, O.: Neuromorphic wireless split computing with multi-level spikes. *IEEE Transactions on Machine Learning in Communications and Networking* **3**, 502–516 (2025)

- [38] Bar, B., Santos, J.P., Uzdin, R.: Layered kik quantum error mitigation for dynamic circuits and error correction. arXiv preprint arXiv:2504.12457 (2025)
- [39] Jang, H., Skatchkovsky, N., Simeone, O.: VOWEL: A local online learning rule for recurrent networks of probabilistic spiking winner-take-all circuits. In: 2020 25th International Conference on Pattern Recognition (ICPR), pp. 4597–4604 (2021). IEEE
- [40] Sannia, A., Giorgi, G.L., Zambrini, R.: Exponential concentration and symmetries in quantum reservoir computing. arXiv preprint arXiv:2505.10062 (2025)
- [41] Spall, J.C.: Multivariate stochastic approximation using a simultaneous perturbation gradient approximation. IEEE transactions on automatic control **37**(3), 332–341 (1992)
- [42] Chen, J., Park, S., Simeone, O.: Knowing when to stop: Delay-adaptive spiking neural network classifiers with reliability guarantees. IEEE Journal of Selected Topics in Signal Processing **19**(1), 88–102 (2025)

Supplementary Information

S1 Prior Work: Quantum Leaky Integrate-And-Fire Neuron

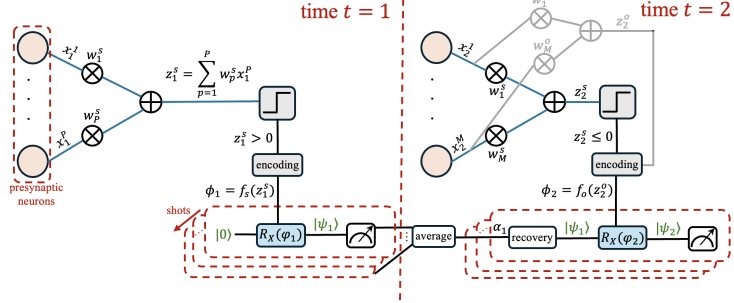


Fig. S1 Supplementary Figure S1. Quantum leaky integrate-and-fire (QLIF) neuron: Schematic of the QLIF neuron with P presynaptic inputs.¹³ A single qubit (green) serves as the neuron’s internal state, evolving in discrete time steps via a measure-and-prepare scheme. At each time t , input spikes from P presynaptic neurons are weighted (blue arrows) and encoded as a rotation ϕ_t on the qubit. The qubit is measured multiple times to estimate a spike probability (red arrow), which is compared against a threshold to decide if the neuron fires. This design requires repeated quantum measurements and uses a classical memory (accumulated threshold voltage), mimicking a leaky integrate-and-fire process.

In this section, we review the quantum leaky integrate-and-fire (QLIF) neuron proposed by the prior work¹³. As illustrated in Fig. S1, a QLIF neuron is modeled via an internal single qubit, which evolves over discrete time $t = 1, 2, \dots$ through a measure-and-prepare mechanism characterized by multi-shot measurements. The state of the qubit serves as the inner state of the spiking neurons. Furthermore, a rotation angle φ_t determines whether the neuron produces a spike or not at time t through a measurement probability evaluated via multiple shots. Consider a QLIF neuron that is fed by P pre-synaptic neurons, at each time t , the QLIF neuron receives an input binary signal $\mathbf{x}_t = [x_t^1, \dots, x_t^P]^T \in \{0, 1\}^P$, with $x_t^p \in \{0, 1\}$ representing the binary activation of the p -th presynaptic neuron. A signal $x_t^p = 1$ indicates the presence of a spike, and $x_t^p = 0$ indicates that the p -th presynaptic neuron does not spike at time t .

The QLIF neuron connects to P presynaptic neurons via two vectors of weights $\mathbf{w}^s = [w_1^s, \dots, w_P^s]^T$ and $\mathbf{w}^o = [w_1^o, \dots, w_P^o]^T$. Specifically, the pre-synaptic signals are aggregated into the input signals

$$z_t^s = \sum_{p=1}^P w_p^s x_t^p, \quad (\text{S1})$$

and

$$z_t^o = \sum_{p=1}^P w_p^o x_t^p. \quad (\text{S2})$$

As in classical neuromorphic computing, the complexity of evaluating the signals (S1) and (S2) is proportional to the number of pre-synaptic spikes. Therefore, sparser input signals reduce the complexity of computing (S1) and (S2).

The signals (S1) and (S2) are used to determine the state of the internal qubit of the QLIF neuron through a rotation angle φ_t . In particular, at each time t , the internal qubit state $|\psi_t\rangle$ is prepared from the ground state $|0\rangle$ via the Pauli X-rotation gate

$$R_X(\varphi_t) = \begin{bmatrix} \cos(\varphi_t/2) & -i \sin(\varphi_t/2) \\ -i \sin(\varphi_t/2) & \cos(\varphi_t/2) \end{bmatrix} \quad (\text{S3})$$

as $|\psi_t\rangle = R_X(\varphi_t)|0\rangle$, where the angle φ_t depends on the input signals (S1)-(S2) as discussed below. A standard measurement of the qubit yields output 1 with probability

$$\alpha_t = |\langle 1|\psi_t\rangle|^2 = (\sin(\varphi_t))^2. \quad (\text{S4})$$

This probability is estimated by preparing and measuring state $|\psi_t\rangle$ multiple times. The probability (S4) represents the counterpart of the membrane potential of classical spiking neurons^{22,42}. In fact, using the estimated probability α_t , a spike is generated if the probability α_t exceeds a predetermined threshold $\vartheta \in [0, 1]$, i.e.,

$$s_t = \begin{cases} 0 \text{ (no spike)}, & \text{if } \alpha_t \leq \vartheta, \\ 1 \text{ (spike)}, & \text{if } \alpha_t > \vartheta. \end{cases} \quad (\text{S5})$$

This signal serves as an input to the post-synaptic neurons connected to the given QLIF neuron for time $t + 1$.

We now describe the evaluation of the phase φ_t used in the rotation (S3). First, at time t , the phase φ_t is first initialized as

$$\varphi_t^o = \begin{cases} 2 \arcsin(\sqrt{\alpha_t}), & \text{if } s_{t-1} = 0, \\ 0, & \text{if } s_{t-1} = 1. \end{cases} \quad (\text{S6})$$

Using (S4), this operation recovers the phase φ_{t-1} if no spike is generated at time $t - 1$, i.e., if $s_{t-1} = 0$. Otherwise, if the QLIF had spiked at the previous time, i.e., $s_{t-1} = 1$, the phase is reset to zero, i.e., $\varphi_t^o = 0$. Having initialized the phase φ_t^o , the rotation angle φ_t is computed as

$$\varphi_t = \varphi_t^o + \phi_t, \quad (\text{S7})$$

where the angle ϕ_t depends on the signals (S1)-(S2) computing from the input spikes. Note that we set $\varphi_0^o = 0$, so that the qubit state at time $t = 1$ is $|\psi_1\rangle = R_X(\varphi_1)|0\rangle = R_X(\phi_1)|0\rangle$.

When the input current z_t^s is positive, the rotation gate applies a positive angle $\phi_t > 0$, exciting the membrane potential and increasing the spiking probability (S4), while otherwise a rotation with a negative angle $\phi_t \leq 0$ is applied, reducing the spiking probability (S4). Thus a positive input current z_t^s causes the QLIF neuron to integrate its inputs, while a negative input current $z_t^s \leq 0$ entails the “leaking” of the membrane potential (S4). Specifically, given the previous spiking probability α_{t-1} , the angle ϕ_t is determined as

$$\phi_t = \begin{cases} f_s(z_t^s), & \text{if } z_t^s > 0, \\ f_o(z_t^o), & \text{if } z_t^s \leq 0, \end{cases} \quad (\text{S8})$$

with $f_s(z_t^s) = \pi z_t^s$ and $f_o(z_t^o) = -2 \arcsin(\sqrt{\alpha_{t-1} \exp(-\beta |z_t^o|/T_1)})$, where $\beta > 0$ is a scaling factor and T_1 is the parameter that controls the rate of decay towards the ground state $|0\rangle$. Reference¹³ optimizes the weights \mathbf{w}^s and \mathbf{w}^o by using the arctan surrogate gradient for the spike generation process (S5) via backpropagation on a classical computer.

S2 Surrogate Gradient Learning for SQSNNs

This section introduces a surrogate gradient-based learning technique enabling the use of backpropagation for a classical simulator of an SQSNN. The approach is inspired by well-established methods for classical SNNs³¹.

To elaborate, we consider a classification task with $|\mathcal{O}|$ classes, where \mathcal{O} is the set of output neurons. Given an input at each time t , the output neurons produce a vector of spikes $\hat{\mathbf{o}}_t = [\hat{o}_{1,t}, \dots, \hat{o}_{|\mathcal{O}|,t}]$, with $\hat{o}_{i,t} \in \{0, 1\}^N$. The spike rate for each output neuron $i \in \mathcal{O}$ over the full sequence of length T is evaluated as $\mathbf{r}_i = \frac{1}{T} \sum_{t=1}^T \hat{o}_{i,t}$, providing an estimate of the spiking probability (16). The loss in (16) is approximated as the cross-entropy between the spike rates \mathbf{r}_i and the target outputs \mathbf{o}_i^T

$$\mathcal{L}(\Theta) = \frac{1}{|\mathcal{B}| |\mathcal{O}| NT} \sum_{\mathbf{o}^T \in \mathcal{B}} \sum_{i=1}^{|\mathcal{O}|} \sum_{n=1}^N \sum_{t=1}^T [-o_{i,t}^n \log(r_i^n) - (1 - o_{i,t}^n) \log(1 - r_i^n)], \quad (\text{S9})$$

where $\mathcal{B} \subseteq \mathcal{D}$ is a mini-batch.

During the forward process, the output $\mathbf{s}_{i,t}$ of each neuron i at each time t is sampled from the Bernoulli distribution with probability $p_{\Theta_i}(\mathbf{s}_{i,t} | \mathbf{s}_{\mathcal{P}_i \cup \{i\}}^{t-1})$. Applying the chain rule, we compute the gradient of the loss (S9) with respect to model parameters Θ_i of each neuron i as

$$\frac{\partial \mathcal{L}(\Theta)}{\partial \Theta_i} = \frac{\partial \mathcal{L}(\Theta)}{\partial \mathbf{s}_{i,t}} \cdot \frac{\partial \mathbf{s}_{i,t}}{\partial p_{\Theta_i}(\mathbf{s}_{i,t} | \mathbf{s}_{\mathcal{P}_i \cup \{i\}}^{t-1})} \cdot \frac{\partial p_{\Theta_i}(\mathbf{s}_{i,t} | \mathbf{s}_{\mathcal{P}_i \cup \{i\}}^{t-1})}{\partial \Theta_i}. \quad (\text{S10})$$

However, the spiking signals $\mathbf{s}_{i,t}$ are random and thus the chain rule (S10) cannot be directly used. To address this problem, we replace the N -dimensional binary random signal $\mathbf{s}_{i,t}$ with a deterministic N -dimensional vector taking values in the interval $[0, 1]$. Specifically, denoting as $\sigma(\cdot)$ the element-wise sigmoid function $\sigma(x) = 1/(1 +$

$\exp(-x)$), we replace vector $\mathbf{s}_{i,t}$ with the surrogate $\sigma(p_{\Theta_i}(\mathbf{s}_{i,t}|\mathbf{s}_{\mathcal{P}_i \cup \{i\}}^{t-1}))$, yielding the partial derivative approximation

$$\frac{\partial \mathcal{L}(\Theta)}{\partial \Theta_i} = \frac{\partial \mathcal{L}(\Theta)}{\partial \mathbf{s}_{i,t}} \cdot \frac{\partial \sigma(p_{\Theta_i}(\mathbf{s}_{i,t}|\mathbf{s}_{\mathcal{P}_i \cup \{i\}}^{t-1}))}{\partial p_{\Theta_i}(\mathbf{s}_{i,t}|\mathbf{s}_{\mathcal{P}_i \cup \{i\}}^{t-1})} \cdot \frac{\partial p_{\Theta_i}(\mathbf{s}_{i,t}|\mathbf{s}_{\mathcal{P}_i \cup \{i\}}^{t-1})}{\partial \Theta_i}. \quad (\text{S11})$$

This approximation is applied during the backward pass of backpropagation to estimate the gradient $\nabla_{\Theta} \mathcal{L}(\Theta)$.

S3 Per-Neuron Spiking Activity

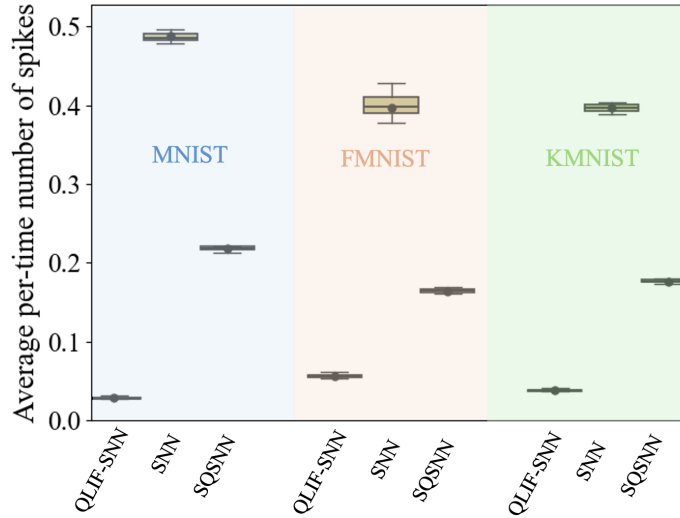


Fig. S2 Supplementary Figure S2. Box plots show the average number of spikes per neuron per time step for the QLIFF-SNN, classical SNN, and SQSNN models across the MNIST, FMNIST, and KMNIST datasets. This figure complements Fig. 2(c) in the main text by normalizing spike activity on a per-neuron basis. All models exhibit sparse spiking behavior (rates well below 1 spike per neuron per time step), with SQSNN striking a balance between the high activity of classical SNNs and the low activity of QLIFF-SNNs.

To clarify the network-level spiking statistics reported in the main manuscript, we provide here the average number of spikes per neuron per time step for each model across the three datasets: MNIST, FMNIST, and KMNIST. This complements Fig. 2(c) in the main text, which shows the total number of spikes per time step aggregated over the entire network. As shown in Fig. S2, The SQSNN’s intermediate per-neuron spiking level reflects a favorable trade-off: sufficient activity to support expressive computation, while maintaining energy-efficient operation. This balance likely contributes to its superior performance-efficiency characteristics, as discussed in the main manuscript.